Transl. Stroke Res. (2015) 6:215–223
DOI 10.1007/s12975-015-0388-8

ORIGINAL ARTICLE

Iron-Induced Necrotic Brain Cell Death in Rats with Different Aerobic Capacity

Mingzhe Zheng · Hanjian Du · Wei Ni · Lauren G. Koch · Steven L. Britton · Richard F. Keep · Guohua Xi · Ya Hua

Received: 5 November 2014 / Revised: 16 January 2015 / Accepted: 21 January 2015 / Published online: 5 February 2015

Abstract Brain iron overload has a key role in brain injury after intracerebral hemorrhage (ICH). Our recent study demonstrated that ICH-induced brain injury was greater in low capacity runner (LCR) than in high capacity runner (HCR) rats. The present study examines whether iron-induced brain injury differs between LCRs and HCRs. Adult male LCR and HCR rats had an intracaudate injection of iron or saline. Rats were euthanized at 2 and at 24 h after T2 magnetic resonance imaging, and the brains were used for immunostaining and Western blotting. LCRs had more hemispheric swelling, T2 lesion volumes, blood-brain barrier disruption, and neuronal death at 24 h after iron injection ($p<0.05$). Many propidium iodide (PI)-positive cells, indicative of necrotic cell death, were observed in the ipsilateral basal ganglia of both HCRs and LCRs at 2 h after iron injection. PI fluorescence intensity was higher in LCRs than in HCRs. In addition, membrane attack complex (MAC) expression was increased at 2 h after iron injection and was higher in LCRs than in HCRs. The PI-positive cells co-localized with MAC-positive cells in the ipsilateral basal ganglia. Iron induces more severe necrotic brain cell death, brain swelling, and blood-brain barrier disruption in LCR rats, which may be related with complement activation and MAC formation.

Keywords Intracerebral hemorrhage · The blood-brain barrier · Membrane attack complex · Necrotic brain cell death

M. Zheng · H. Du · W. Ni · R. F. Keep · G. Xi · Y. Hua (✉)
Department of Neurosurgery, University of Michigan, R5018 BSRB, 109 Zina Pitcher Place, Ann Arbor, MI 48109-2200, USA
e-mail: yahua@umich.edu

L. G. Koch · S. L. Britton
Department of Anesthesiology, University of Michigan, Ann Arbor, MI, USA

Introduction

Iron has a major role in intracerebral hemorrhage (ICH)-induced brain injury [1–3]. The breakdown of hemoglobin during intracerebral hematoma resolution results in a buildup in perihematomal iron. Thus, we showed a significant increase in brain non-heme iron after ICH in rats, and this remains high for at least 1 month [4]. Brain iron overload causes brain edema in the acute phase and brain atrophy later after ICH [4–6]. We have demonstrated that the iron chelator, deferoxamine, reduces ICH-induced brain edema, neuronal death, brain atrophy, and neurological deficits in young rats [7–9], aged rats [10, 11], and pigs [12].

Complement-mediated brain injury has been found in many central nervous system diseases, including neurodegenerative disorders, traumatic brain injury, cerebral ischemia, and ICH [13–17]. Our previous studies have demonstrated that complement depletion or complement inhibition reduces perihematomal brain edema in a rat model of ICH [15, 16]. ICH results in less brain injury in complement C3-deficient mice [18]. Complement activation is an important contributor to tissue necrosis following ischemia [19, 20]. The membrane attack complex (MAC), the terminal complement pathway and composed of C5b-9, induces a necrotic cell death [21].

Low exercise capacity is a risk factor for stroke [22] as well as other forms of cardiovascular disease [23–25]. Using rats bred for low and high aerobic capacity [26], we recently showed that the low capacity runner (LCR) rats had more severe ICH-induced brain injury than the high capacity runners (HCR), including worse brain edema, brain atrophy, and neurological deficits [26]. We hypothesized that the differences in ICH-induced brain injury with aerobic capacity relate to differences in susceptibility to iron-induced injury. Therefore, in the present study, we examined if iron-induced injury differs between LCR and HCR rats, focusing on necrotic brain

cell death, MAC formation, brain swelling, and blood-brain barrier (BBB) disruption.

Materials and Methods

Animal Preparation and Intracerebral Infusion

All animal procedures were approved by the University Committee on Use and Care of Animals, University of Michigan. The detailed description on the development of different aerobic capacity rats has been described previously [27]. Adult male HCR and LCR rats (generations 31 and 32) were anesthetized with pentobarbital (45 mg/kg, i.p.), and the right femoral artery was catheterized to monitor arterial blood pressure, blood pH, PaO_2, $PaCO_2$, hematocrit, and glucose levels. Body temperature was maintained at 37.5 °C by a feedback-controlled heating pad. The animals were then positioned in a stereotactic frame and injections administered into the right basal ganglia (coordinates at 0.2 mm anterior to bregma, 5.5 mm ventral, and 3.5 mm lateral to midline). Fifty microliters of $FeCl_2$ (0.5 mM) or saline was infused at 5 μl/min using a microinfusion pump. After injection, the needle was removed and the skin incisions closed.

Experimental Groups

The present study was divided into two parts. In the first part, HCR (n=10) and LCR (n=10) rats had 50 μl of $FeCl_2$ (0.5 mmol/L) infused into the right caudate. T2 magnetic resonance imaging was performed at 24 h after iron injection (n=6 for each group), and the rats were then used for brain histology and Western blotting. In the second part, HCRs (n=6) and LCRs (n=6) had an intracaudate infusion of 50 μl of $FeCl_2$ (0.5 mmol/L) with propidium iodide (PI, 0.04 mg/mL). In addition, control HCRs and LCRs (n=3) had an intracaudate infusion of 50 μl saline with PI. All rats were euthanized after 2 h for immunohistochemistry and Western blotting.

Table 1 Aerobic capacity data and body weight for HCR and LCR rats in this study

	Body weight (g)	Best time (min)	Best distance (m)	Best speed (m/min)	Vertical work (J)
HCR (n=19)	368±37	74.7±5.2	2109±241	46.8±2.7	1315±102
LCR (n=16)	464±65	13.5±1.9	175±30	16.3±1.1	142±27
p value	<0.01	<0.01	<0.01	<0.01	<0.01

Values are means±SD

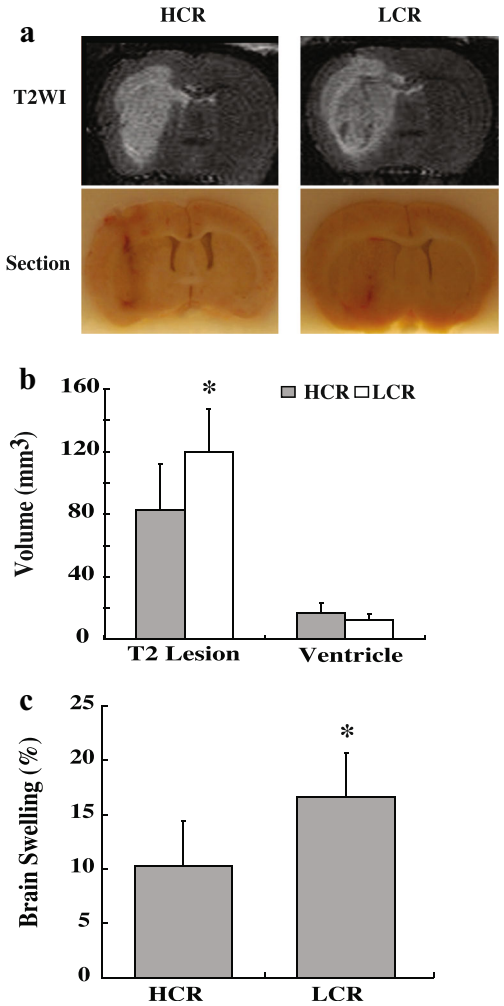

Fig. 1 Representative T2-weighted MRI images with corresponding coronal sections (**a**) and measurements of lesion and ventricular volume (**b**) and brain swelling (**c**) in HCR and LCR rats 24 h after injection of 50 μl $FeCl_2$ (0.5 mM) into the right caudate. Values are mean±SD; n=6, *p<0.05 vs. HCR

Magnetic Resonance Imaging and Volume Measurement

Imaging was carried out in a 7.0-T Varian MR scanner (183-mm horizontal bore; Varian, Palo Alto, CA) at the Center for Molecular Imaging (CMI) of the University of Michigan. Rats were anesthetized with 2 % isoflurane/air mixture throughout MRI examination. The imaging protocol for all rats included a T2 fast spin-echo sequence (TR/TE=4000/60 msec). The

Fig. 2 Albumin immunoreactivity in coronal sections (**a**) and albumin ▶ protein levels in the ipsilateral basal ganglia (**b**) in HCRs and LCRs 24 h after $FeCl_2$ injection into the right caudate. Albumin protein levels are expressed as the pixel ratio to β-actin. Scale bar=2.0 mm. Values are mean±SD; n=4, $^{\#}p$<0.01 vs. HCR contralateral basal ganglia, *p<0.05 vs. LCR ipsilateral basal ganglia

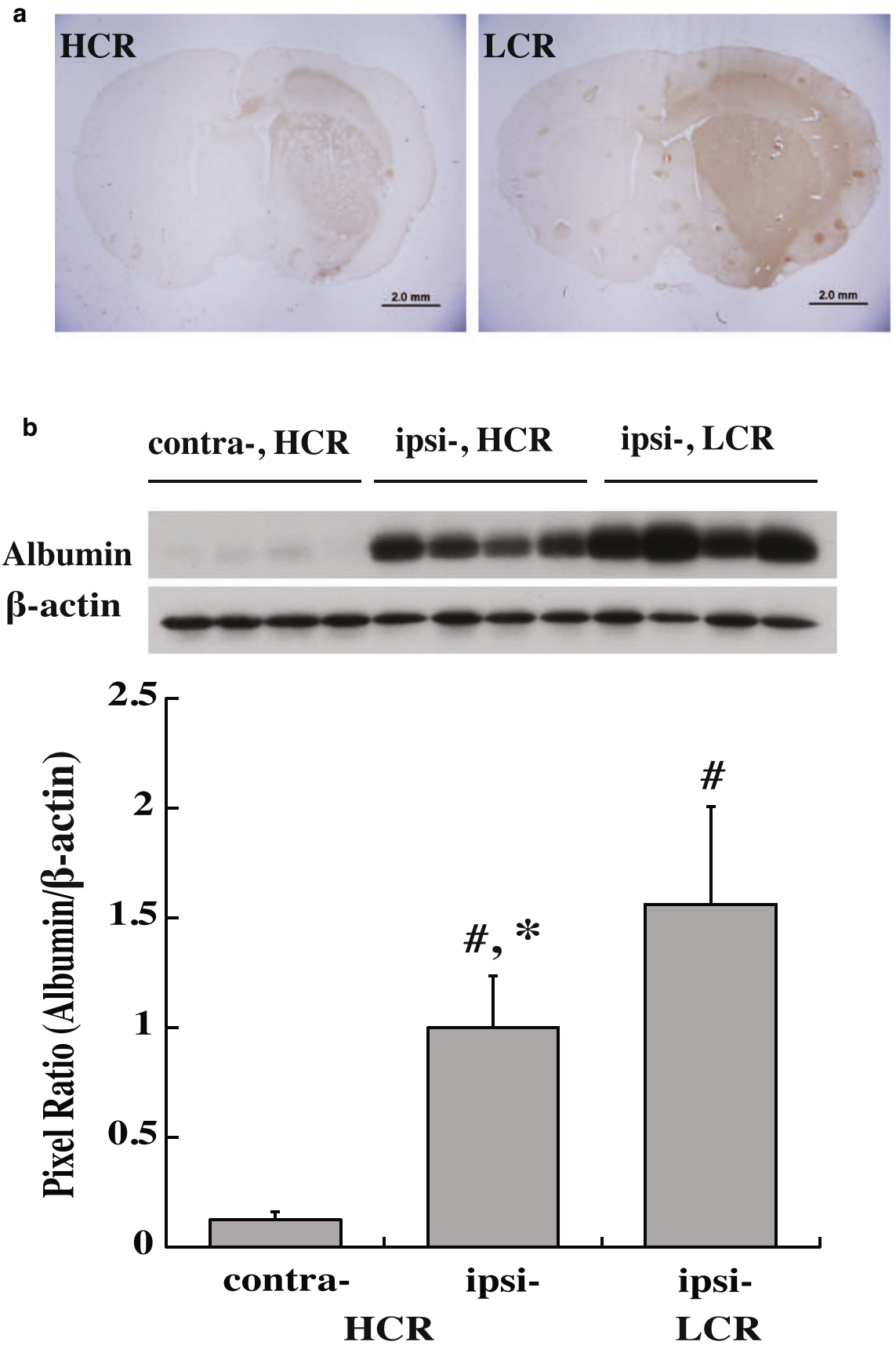
a
HCR
LCR
2.0 mm
2.0 mm
b
contra-, HCR
ipsi-, HCR
ipsi-, LCR
Albumin
β-actin
Pixel Ratio (Albumin/β-actin)
2.5
2
1.5
1
0.5
0
#, *
#
contra-
HCR
ipsi-
ipsi-
LCR

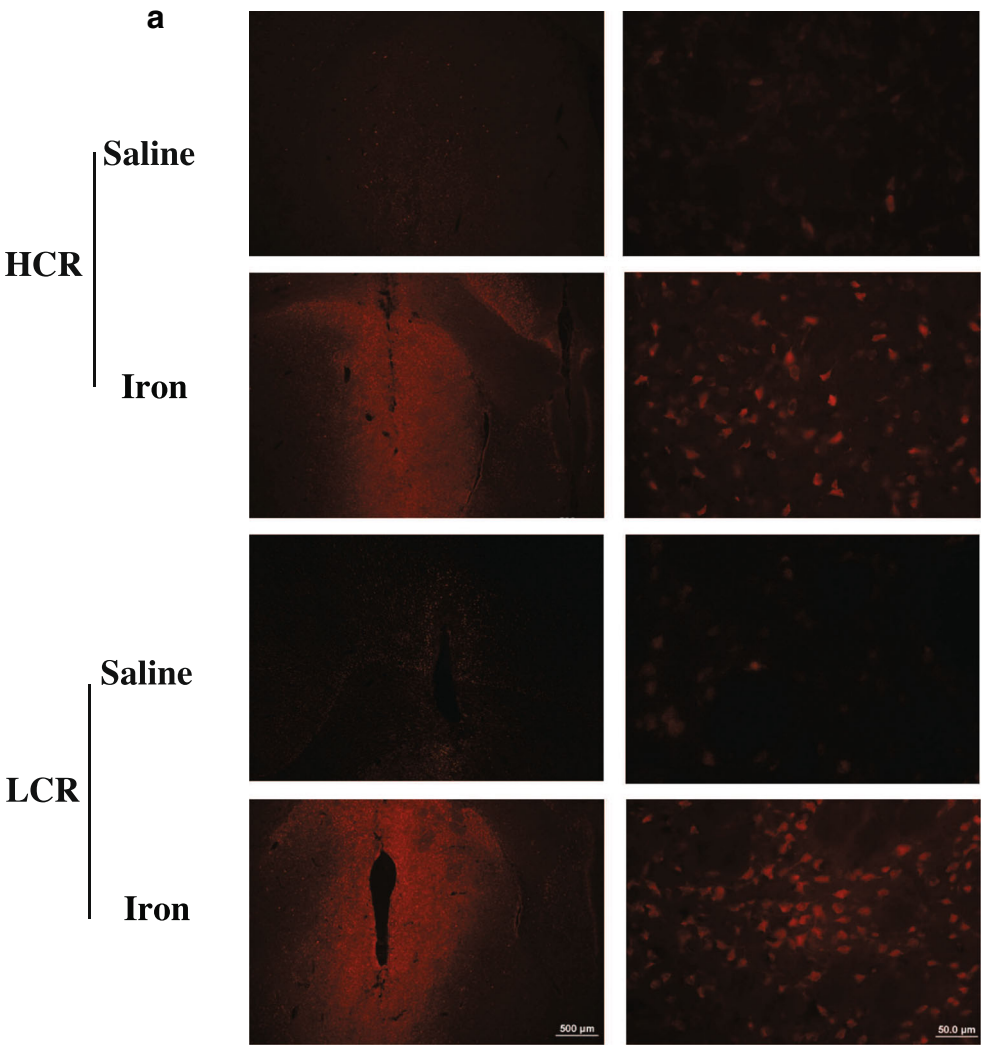
a
Saline
HCR
Iron
Saline
LCR
Iron
500 μm
50.0 μm

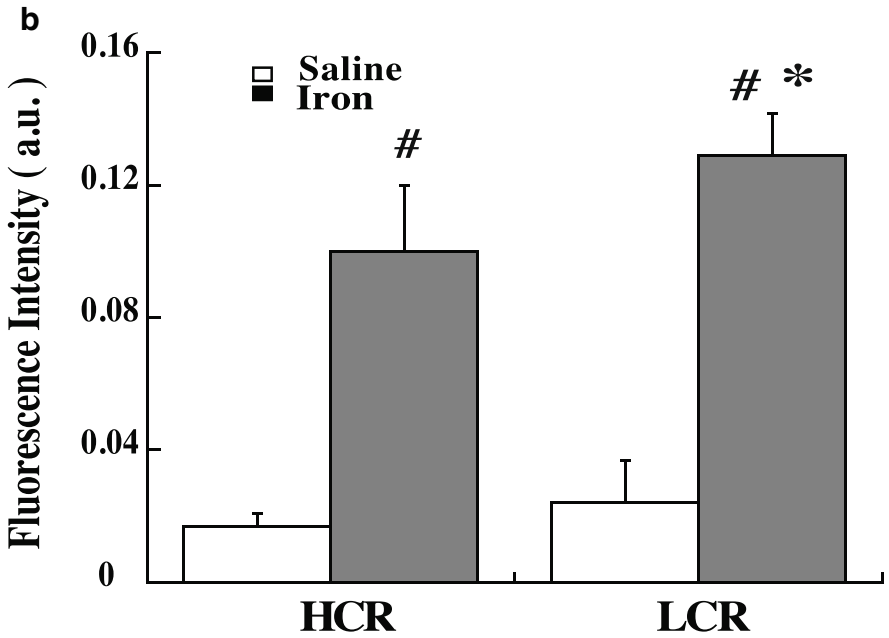
b
Fluorescence Intensity (a.u.)
0.16
0.12
0.08
0.04
0
Saline
Iron
#
*
HCR
LCR

◀ **Fig. 3** **a** Propidium iodide (PI) staining and **b** fluorescence intensity in the ipsilateral basal ganglia of HCR and LCR rats 2 h after an injection of 50 μl of saline or $FeCl_2$ (0.5 mM) with PI (0.04 mg/mL) into the right caudate. Values are mean±SD; $n=3$, $^{\#}p<0.01$ vs. saline group, $^{*}p<0.05$ vs. HCR iron group. Scale bars=500 μm (*left*) or 50 μm (*right*)

images were preserved as 256×256 pixels pictures, and lesion volume, brain swelling, and ventricle volume were measured by NIH ImageJ. Volume measurements were carried out by a blinded observer. Lesion volume was calculated as total lesion volume of all lesion-visible sections. Brain swelling calculation was based upon seven every other sections whose center was the anterior commissure layer; the value was (volume of ipsilateral hemisphere − volume of contralateral hemisphere)/volume of contralateral hemisphere×100 %. Ventricle volume was calculated as the total volume of lateral ventricles.

Immunohistochemistry and Immunofluorescent Staining

Immunohistochemistry was performed as described previously [28]. Briefly, rats were anesthetized and subjected to intracardiac perfusion with 4 % paraformaldehyde in 0.1 mM phosphate-buffered saline (pH 7.4). Brains were removed and kept in 4 % paraformaldehyde for 6 h, then immersed in 30 % sucrose for 3–4 days at 4 °C. After embedding in a mixture of 30 % sucrose and OCT, 18-μm sections were cut on a cryostat. For immunohistochemistry, the primary antibody was goat anti-albumin antibody (Bathyl Laboratories, Inc., 1:600 dilution) and mouse anti-C5b-9 antibody (Abcam, 1:300 dilution). For immunofluorescence, the primary antibody was mouse anti-C5b-9 antibody (Abcam, 1:300 dilution) and the secondary antibody was Alexa Fluro 488-conjugated donkey anti-mouse mAb (Invitrogen, 1:500 dilution).

Western Blot Analysis

Western blot analysis was performed as previously described [28]. Briefly, brain tissue was immersed in Western sample buffer and sonicated. Protein concentration was determined by Bio-Rad protein assay kit, and 50 μg protein samples were separated by sodium dodecyl sulfate-polyacrylamide gel electrophoresis and transferred to a Hybond-C pure nitrocellulose membrane (Amersham). Membranes were probed with goat anti-albumin antibody (Bathyl Laboratories, Inc., 1:10000 dilution) and mouse anti-C5b-9 antibody (abcam, 1:1000 dilution). The antigen–antibody complexes were visualized with the ECL chemiluminescence system (Amersham) and exposed to Kodak X-OMAT film. The relative densities of bands were analyzed with NIH ImageJ.

Fluoro-Jade C Staining

Brain sections were kept in 0.06 % potassium permanganate for 15 min and rinsed in distilled water. Sections were then stained by gently shaking for 30 min in working solution of Fluoro-Jade C composed of 10 mL 0.01 % Fluoro-Jade C in distilled water and 90 mL 0.1 % acetic acid and then rinsed in distilled water three times. After being dried with a blower, slides were quickly dipped into xylol and covered after being mounted by DPX (Electron Microscopy Sciences, Inc.).

Cell Counting and Fluorescence Intensity Measurement

Counting of positive cells and fluorescence intensity measurement was performed on brain coronal sections. Five high-power (×40) fields (center, upper, lower, medial, and lateral parts of the lesion in basal ganglia) were taken using a digital

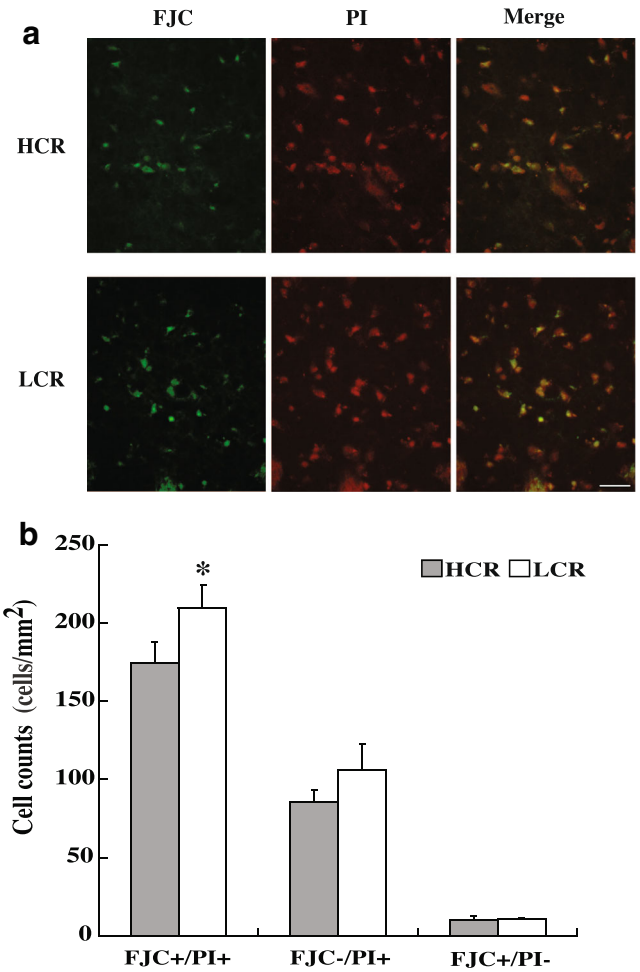

Fig. 4 **a** Fluoro-Jade C (*FJC*, *green*) and propidium iodide (*PI*, *red*) staining and their co-localization (*yellow*) in the ipsilateral basal ganglia of HCRs and LCRs at 2 h after $FeCl_2$ injection. **b** The number of cells positive for either Fluoro-Jade C or propidium iodide alone (FJC+/PI−, FJC−/PI+) or both (FJC+/PI+). Scale bar=50 μm. Values are means±SD; $n=3$, $^{*}p<0.05$ vs. HCR

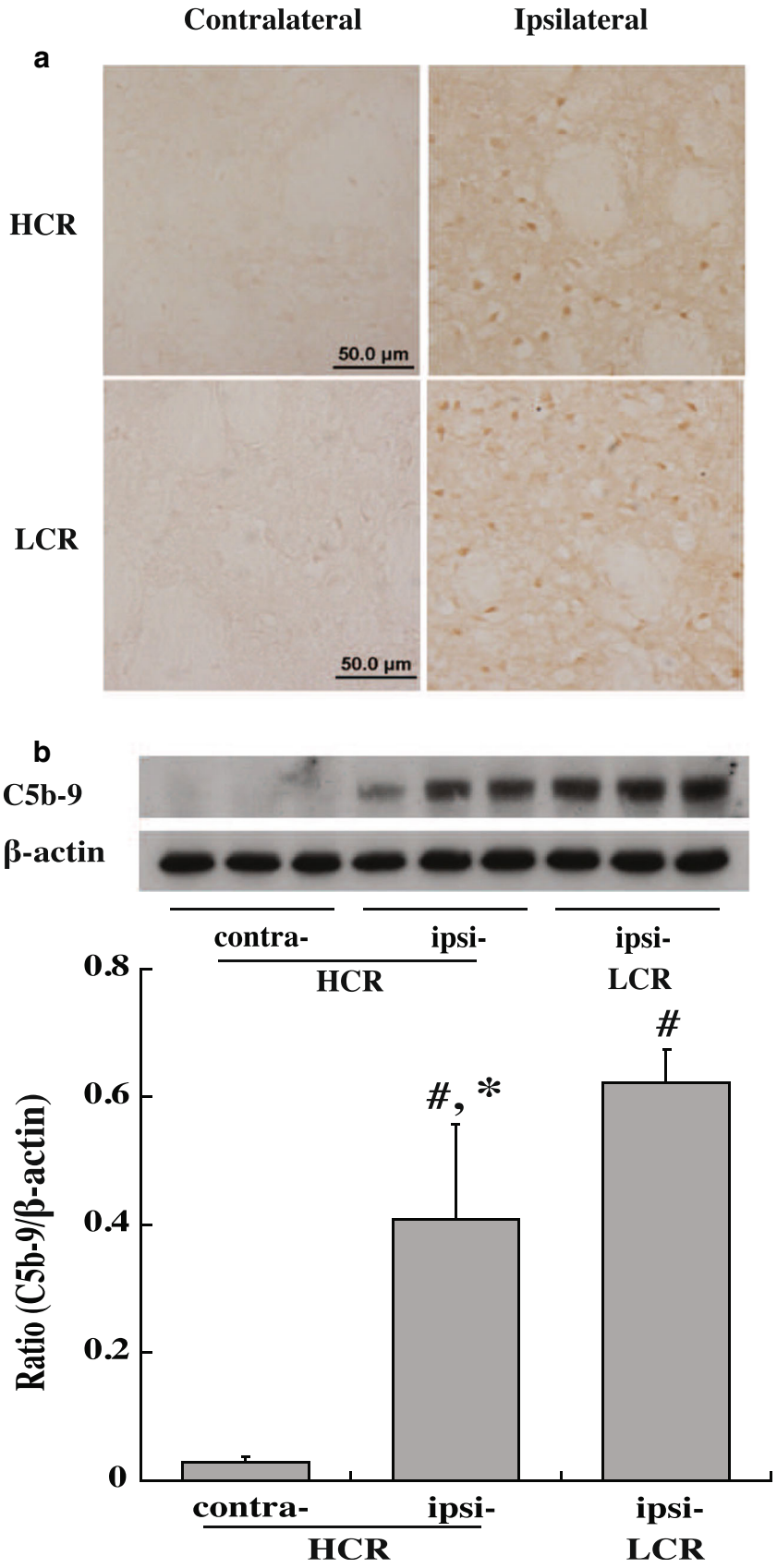
Contralateral
Ipsilateral
a
HCR
LCR
50.0 μm
50.0 μm
b
C5b-9
β-actin
contra-
ipsi-
HCR
ipsi-
LCR
Ratio (C5b-9/β-actin)
0.8
0.6
0.4
0.2
0
#, *
#
contra-
ipsi-
HCR
ipsi-
LCR

◀ **Fig. 5** a C5b-9 immunoreactivity in the caudate of HCRs and LCRs at 2 h after $FeCl_2$ injection. **b** Quantification of complement 5b-9 protein levels by Western blotting (expressed as ratio to β-actin). Values are mean±SD; $n=3$, $^{\#}p<0.01$ vs. HCR contralateral basal ganglia, $^{*}p<0.05$ vs. LCR ipsilateral basal ganglia

camera. Four layers at approximately same distance to the injection site were selected for each section. Plasmalemma permeability to PI is associated with markers of cell death as shown in ischemic, traumatic brain injury and ICH models [29–31]. It was used as a marker of neuronal death in our ICH model [32]. The relative fluorescence intensity was analyzed by NIH ImageJ. Cell counts were performed by a blinded observer. All measurements were repeated three times, and the mean value was used.

Statistical Analysis

All the data in this study are presented as mean±SD. Data were analyzed by Student's *t* test or ANOVA test. Differences were considered significant at $p<0.05$.

Results

Physiological Parameters

The mean distance run at exhaustion, calculated from time (min) and speed (m/min), was higher in HCRs than in LCRs (2109±241 vs. 175±30 m, $p<0.01$). The HCRs could perform about eightfold more vertical work than LCRs (1315±102 vs. 142±27 J, $p<0.01$; Table 1).

At the time of surgery, LCRs were significantly heavier than HCRs (464±65 vs. 368±37 g, $p<0.01$). Blood pressure, glucose, hematocrit, pH, PaO_2, and $PaCO_2$ were all in normal ranges. No rats were found dead postoperatively.

Intracaudate Injection of Iron Resulted in Larger Lesion Volumes and Severe Brain Swelling in LCR Rats

T2 lesions were larger in LCRs (120.1±27.5 vs. 82.5±30.2 mm^3 in HCRs, $p<0.05$) at 24 h after iron infusion (Fig. 1a, b). There was more severe brain swelling (% of ipsilateral–contralateral/contralateral hemispheric volumes on MRI) in LCRs (16.6±4.1 %) compared to HCRs (10.3±4.2 %, $p<0.05$; Fig. 1a, c). While intracaudate injection of iron caused severe caudate injury, it also affected the corpus callosum and cortex. The lateral ventricle volumes were similar (12.6±4.0 mm^3 in LCRs vs. 16.8±6.1 mm^3 in HCRs, $p>0.05$).

Iron Caused More Severe BBB Leakage and Neuronal Death in LCRs

The area staining for albumin in the ipsilateral hemisphere was larger in LCRs than in HCRs 24 h after iron injection (Fig. 2a). Albumin levels were very low in the contralateral caudate of HCRs (ratio to β-actin, 0.12±0.04; Fig. 2b) and was significantly increased after iron injection (1.00±0.23, $p<0.01$ vs. contralateral). Albumin levels were much higher in the ipsilateral caudate of LCRs than in HCRs (1.56±0.45 vs. 1.00±0.23, $p<0.05$; Fig. 2b).

The number of Fluoro-Jade C-positive cells (dying neurons) was significantly higher in the ipsilateral basal ganglia of LCRs (231±28 vs. 185±24 cells/mm^2 in HCRs, $p<0.05$) at 24 h after the injection of iron.

Iron Caused Ultra-Early Necrotic Neuronal Death

PI-positive cells were found in the ipsilateral caudate and adjacent cortex 2 h after iron injection, but not saline injection (Fig. 3a). PI fluorescence intensity in the ipsilateral basal ganglia after iron injection was significantly higher in the LCRs (0.13±0.01 vs. 0.10±0.02 in HCRs, $p<0.05$). There was little PI fluorescence after saline injection (Fig. 3b).

Fluoro-Jade C-positive cells were mostly located near the injection site at 2 h after iron injection. Fluoro-Jade C-positive cells in the ipsilateral caudate of both HCRs and LCRs were mostly also positive for PI (Fig. 4a) at 2 h. The ratio of (FJC^+/PI^+)/PI^+ was 67±2 % in HCRs and 67±4 % in LCRs, indicating that the majority of ultra-acute necrotic cells were neurons. The number of FJC^+/PI^+ cells was significantly higher in the ipsilateral basal ganglia of LCRs (210±14 vs. 174±14 cells/mm^2 in HCRs; Fig. 4b). The number of FJC^-/PI^+ cells was the

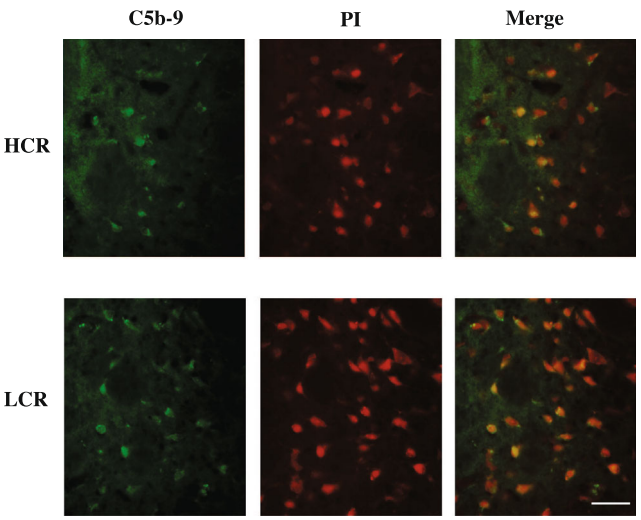

Fig. 6 Co-localization of C5b-9 immunoreactivity with PI-positive cells in the ipsilateral basal ganglia of HCRs and LCRs at 2 h after $FeCl_2$ injection. Scale bar=50 μm

same in LCRs and HCRs. There were few FJC^+/PI^- cells in both LCRs and HCR rats.

Iron-Induced Ultra-Early MAC Formation

Two hours after iron injection, C5b-9-positive cells were mostly detected in the ipsilateral basal ganglia in both HCRs and LCRs. Almost no C5b-9 was detected in the contralateral basal ganglia of HCRs and LCRs. There were more C5b-9-positive cells in the ipsilateral basal ganglia of LCR compared to HCR rats (Fig. 5a). The protein levels of C5b-9 were much higher in the ipsilateral basal ganglia of HCRs (ratio to β-actin, 0.41± 0.15) compared to the contralateral side (0.03±0.01, $p<0.01$; Fig. 5b). C5b-9 protein levels were also significantly higher in the ipsilateral basal ganglia of LCRs (ratio to β-actin, 0.62±0.05) compared to HCRs (0.41± 0.15, $p<0.05$; Fig. 5b). C5b-9-positive cells were neuron-like and co-localized with PI-positive cells (Fig. 6).

Discussion

The major findings of the present study are: (1) Iron injection resulted in ultra-early necrotic brain cell death. (2) Iron caused ultra-early MAC formation in the brain which may result in necrotic cell death. (3) LCRs had more severe iron-induced brain swelling, BBB leakage, neuronal death, and MAC formation than HCRs. These results suggest that targeting iron overload and complement activation may be particularly important in the setting of low aerobic capacity.

Iron has an important role in ICH-induced brain injury, and the precise mechanisms of iron-induced neuronal death need to be studied further. Most research has focused on oxidative injury. Reactive oxygen species contribute to DNA and protein structure damage. After ICH, perihematomal iron concentrations increase, peaking at 7–14 days [4, 5]. Therefore, iron chelators have been used to alleviate oxidative damage following ICH [6]. Recently, the term "ferroptosis" was adopted to describe a new type of cell death related to iron, which differs from apoptosis and autophagy [33]. Necroptosis can also be related to iron [34, 35]. Our study indicates that iron causes significant necrotic brain cell death.

MAC formation is a terminal procedure of complement system activation, which may cause necrotic cell death. After assembly and binding to the cell surface, MAC forms a trans-membrane pore that can cause cell lysis. C1q, a complement system component, has increased binding to IgG and IgM when exposed to ferrous iron [36]. Another complement pathway component, C5, can be activated into C5b-like C5 by H_2O_2 [37], especially via binding with iron [38]. These findings indicate that iron may be a potential regulator of the complement system, as suggested by the current study, where intracerebral injection of iron induced MAC formation. As brain iron overload occurs following ICH, downstream MAC formation could be a new therapeutic target for ICH.

In the present study, C5b-9 was expressed in PI-positive cells suggesting that complement activation and MAC formation may contribute to the necrotic cell death following iron injection. The time window of complement system activation after iron injection was 2 h or less, indicating a rapid response. Complement system activation as fast as 10–15 min has been reported after onset of hemodialysis treatment [39]. Both classic and alternative pathways can be involved in activation [40].

Previously, we found that ICH-induced brain injury is greater in LCR rats than HCRs [26]. The current study indicates that iron-induced injury is also greater in LCRs. Differences in iron-mediated injury may underlie the differential susceptibility of LCRs to ICH-induced injury as iron overload contributes to brain injury after ICH [3]. While there may be multiple mechanisms underlying the difference in iron-induced injury with aerobic capacity, the current study demonstrates that iron causes greater complement activation with MAC formation in the brain of LCR rats.

There is evidence that complement activation differs between athletes and sedentary individuals. Thus, the levels of complement C3 and C4 at rest and during exercise and recovery were all lower in athletes than in sedentary groups [41]. In addition, C3 and C4 levels are decreased at the end of aerobic exercise on a treadmill for 30 min [42]. Taken together, these results indicate a potential role of aerobic exercise in regulating complement system activation. The results from the current study support this concept with iron-induced C5b-9 formation being lower in HCR rats than LCRs. These differences in complement components may relate to the effects of exercise on cortisol levels [42], although the underlying mechanism is not clear.

In conclusion, intracerebral iron results in more brain cell necrosis in rats with low intrinsic aerobic capacity (LCRs) than those with a high capacity (HCRs). Complement system activation and MAC formation may contribute to ultra-early necrotic cell death after iron injection.

Acknowledgments This study was supported by grants NS-073595, NS-079157, NS-084049, OD-010950, DK-077200 and GM-104194 from the National Institutes of Health (NIH).

Conflict of Interest Mingzhe Zheng, Hanjian Du, Wei Ni, Lauren G. Koch, Steven L. Britton, Richard F. Keep, Guohua Xi, and Ya Hua declare that they have no conflict of interest.

Compliance with Ethics Requirements All institutional and national guidelines for the care and use of laboratory animals were followed.

References

1. Wagner KR, Sharp FR, Ardizzone TD, Lu A, Clark JF. Heme and iron metabolism: role in cerebral hemorrhage. J Cereb Blood Flow Metab. 2003;23(6):629–52.
2. Xi G, Keep RF, Hoff JT. Mechanisms of brain injury after intracerebral haemorrhage. Lancet Neurol. 2006;5(1):53–63.
3. Keep RF, Hua Y, Xi G. Intracerebral haemorrhage: mechanisms of injury and therapeutic targets. Lancet Neurol. 2012;11(8):720–31.
4. Wu J, Hua Y, Keep RF, Nakamura T, Hoff JT, Xi G. Iron and iron-handling proteins in the brain after intracerebral hemorrhage. Stroke. 2003;34(12):2964–9.
5. Hua Y, Keep RF, Hoff JT, Xi G. Brain injury after intracerebral hemorrhage: the role of thrombin and iron. Stroke. 2007;38(2 Suppl):759–62.
6. Zhao F, Hua Y, He Y, Keep RF, Xi G. Minocycline-induced attenuation of iron overload and brain injury after experimental intracerebral hemorrhage. Stroke. 2011;42(12):3587–93.
7. Nakamura T, Keep RF, Hua Y, Schallert T, Hoff JT, Xi G. Deferoxamine-induced attenuation of brain edema and neurological deficits in a rat model of intracerebral hemorrhage. J Neurosurg. 2004;100(4):672–8.
8. Hua Y, Nakamura T, Keep RF, Wu J, Schallert T, Hoff JT, et al. Long-term effects of experimental intracerebral hemorrhage: the role of iron. J Neurosurg. 2006;104(2):305–12.
9. Song S, Hua Y, Keep RF, Hoff JT, Xi G. A new hippocampal model for examining intracerebral hemorrhage-related neuronal death: effects of deferoxamine on hemoglobin-induced neuronal death. Stroke. 2007;38(10):2861–3.
10. Okauchi M, Hua Y, Keep RF, Morgenstern LB, Xi G. Effects of deferoxamine on intracerebral hemorrhage-induced brain injury in aged rats. Stroke. 2009;40(5):1858–63.
11. Okauchi M, Hua Y, Keep RF, Morgenstern LB, Schallert T, Xi G. Deferoxamine treatment for intracerebral hemorrhage in aged rats: therapeutic time window and optimal duration. Stroke. 2010;41(2):375–82.
12. Gu Y, Hua Y, Keep RF, Morgenstern LB, Xi G. Deferoxamine reduces intracerebral hematoma-induced iron accumulation and neuronal death in piglets. Stroke. 2009;40(6):2241–3.
13. Stahel PF, Morganti-Kossmann MC, Kossmann T. The role of the complement system in traumatic brain injury. Brain Res Rev. 1998;27(3):243–56.
14. Huang J, Kim LJ, Mealey R, Marsh Jr HC, Zhang Y, Tenner AJ, et al. Neuronal protection in stroke by an sLex-glycosylated complement inhibitory protein. Science. 1999;285(5427):595–9.
15. Hua Y, Xi G, Keep RF, Hoff JT. Complement activation in the brain after experimental intracerebral hemorrhage. J Neurosurg. 2000;92(6):1016–22.
16. Xi G, Hua Y, Keep RF, Younger JG, Hoff JT. Systemic complement depletion diminishes perihematomal brain edema in rats. Stroke. 2001;32(1):162–7.
17. Gasque P, Neal JW, Singhrao SK, McGreal EP, Dean YD, Van BJ, et al. Roles of the complement system in human neurodegenerative disorders: pro-inflammatory and tissue remodeling activities. Mol Neurobiol. 2002;25(1):1–17.
18. Yang S, Nakamura T, Hua Y, Keep RF, Younger JG, Hoff JT, et al. Intracerebral hemorrhage in complement C3-deficient mice. Acta Neurochir Suppl. 2006;96:227–31.
19. Walport MJ. Complement. First of two parts. N Engl J Med. 2001;344(14):1058–66.
20. Walport MJ. Complement. Second of two parts. N Engl J Med. 2001;344(15):1140–4.
21. Ziporen L, Donin N, Shmushkovich T, Gross A, Fishelson Z. Programmed necrotic cell death induced by complement involves a Bid-dependent pathway. J Immunol. 2009;182(1):515–21.
22. Kurl S, Sivenius J, Makikallio TH, Rauramaa R, Laukkanen JA. Exercise workload, cardiovascular risk factor evaluation and the risk of stroke in middle-aged men. J Intern Med. 2009;265(2):229–37.
23. Kavanagh T, Mertens DJ, Hamm LF, Beyene J, Kennedy J, Corey P, et al. Peak oxygen intake and cardiac mortality in women referred for cardiac rehabilitation. J Am Coll Cardiol. 2003;42(12):2139–43.
24. Myers J, Prakash M, Froelicher V, Do D, Partington S, Atwood JE. Exercise capacity and mortality among men referred for exercise testing. N Engl J Med. 2002;346(11):793–801.
25. Kokkinos P, Myers J, Kokkinos JP, Pittaras A, Narayan P, Manolis A, et al. Exercise capacity and mortality in black and white men. Circulation. 2008;117(5):614–22.
26. He Y, Liu W, Koch LG, Britton SL, Keep RF, Xi G, et al. Susceptibility to intracerebral hemorrhage-induced brain injury segregates with low aerobic capacity in rats. Neurobiol Dis. 2012;49C:22–8.
27. Wisloff U, Najjar SM, Ellingsen O, Haram PM, Swoap S, Al-Share Q, et al. Cardiovascular risk factors emerge after artificial selection for low aerobic capacity. Science. 2005;307(5708):418–20.
28. Xi G, Keep RF, Hua Y, Xiang J, Hoff JT. Attenuation of thrombin-induced brain edema by cerebral thrombin preconditioning. Stroke. 1999;30(6):1247–55.
29. Unal-Cevik I, Kilinc M, Can A, Gursoy-Ozdemir Y, Dalkara T. Apoptotic and necrotic death mechanisms are concomitantly activated in the same cell after cerebral ischemia. Stroke. 2004;35(9):2189–94.
30. Whalen MJ, Dalkara T, You Z, Qiu J, Bermpohl D, Mehta N, et al. Acute plasmalemma permeability and protracted clearance of injured cells after controlled cortical impact in mice. J Cereb Blood Flow Metab. 2008;28(3):490–505.
31. Zhu X, Tao L, Tejima-Mandeville E, Qiu J, Park J, Garber K, et al. Plasmalemma permeability and necrotic cell death phenotypes after intracerebral hemorrhage in mice. Stroke. 2012;43(2):524–31.
32. Jin H, Xi G, Keep RF, Wu J, Hua Y. DARPP-32 to quantify intracerebral hemorrhage-induced neuronal death in basal ganglia. Transl Stroke Res. 2013;4(1):130–4.
33. Dixon SJ, Lemberg KM, Lamprecht MR, Skouta R, Zaitsev EM, Gleason CE, et al. Ferroptosis: an iron-dependent form of nonapoptotic cell death. Cell. 2012;149(5):1060–72.
34. Dixon SJ, Stockwell BR. The role of iron and reactive oxygen species in cell death. Nat Chem Biol. 2014;10(1):9–17.
35. Dai MC, Zhong ZH, Sun YH, Sun QF, Wang YT, Yang GY, et al. Curcumin protects against iron induced neurotoxicity in primary cortical neurons by attenuating necroptosis. Neurosci Lett. 2013;536:41–6.
36. Dimitrov JD, Roumenina LT, Doltchinkova VR, Vassilev TL. Iron ions and haeme modulate the binding properties of complement subcomponent C1q and of immunoglobulins. Scand J Immunol. 2007;65(3):230–9.
37. von Zabern WV, Hesse D, Nolte R, Haller Y. Generation of an activated form of human C5 (C5b-like C5) by oxygen radicals. Immunol Lett. 1987;14(3):209–15.
38. Vogi W, Nolte R, Brunahl D. Binding of iron to the 5th component of human complement directs oxygen radical-mediated conversion to specific sites and causes nonenzymic activation. Complement Inflamm. 1991;8(5–6):313–9.
39. Lhotta K, Wurzner R, Kronenberg F, Oppermann M, Konig P. Rapid activation of the complement system by cuprophane depends on complement component C4. Kidney Int. 1998;53(4):1044–51.
40. Kourtzelis I, Markiewski MM, Doumas M, Rafail S, Kambas K, Mitroulis I, et al. Complement anaphylatoxin C5a contributes to hemodialysis-associated thrombosis. Blood. 2010;116(4):631–9.
41. Nieman DC, Tan SA, Lee JW, Berk LS. Complement and immunoglobulin levels in athletes and sedentary controls. Int J Sports Med. 1989;10(2):124–8.
42. Karacabey K, Saygin O, Ozmerdivenli R, Zorba E, Godekmerdan A, Bulut V. The effects of exercise on the immune system and stress hormones in sportswomen. Neuroendocrinol Lett. 2005;26(4):361–6.